Synthesis and characterisation of dual plasmonic gold nanostars as high-performance surface-enhanced Raman spectroscopy substrate

Vijay Raghavan[1] ✉, *Hai Ming Fan*[2], *Eoin K. McCarthy*[3], *Peter Dockery*[4], *Antony Wheatley*[5], *Ivan Keogh*[6], *Malini Olivo*[1,7,8]

[1]*School of Physics, National University of Ireland, Galway, Ireland*
[2]*School of Chemical Engineering, Northwest University, Xi'an, People's Republic of China*
[3]*Advanced Microscopy Laboratory, Centre for Research on Adaptive Nanostructures and Nanodevices (CRANN), Trinity College Dublin, Dublin, Ireland*
[4]*Anatomy, National University of Ireland, Galway, Ireland*
[5]*Physiology, National University of Ireland, Galway, Ireland*
[6]*Department of Surgery, National University of Ireland, Galway, Ireland*
[7]*Royal College of Surgeons (RCSI), Dublin, Ireland*
[8]*Bio-optical Imaging Group, Singapore Bioimaging Consortium, Agency for Science, Technology and Research, Singapore*
✉ *E-mail: v.parthasarathy1@nuigalway.ie*

Published in Micro & Nano Letters; Received on 24th March 2016; Revised on 4th August 2016; Accepted on 15th August 2016

Synthesising gold nanoprobes in the near infrared (NIR) region is of particular interest in developing nanosensors due to the minimal light attenuation from biomolecules. Here, the controlled synthesis and tunability of gold nanostars' two distinct localised surface plasmon resonances (LSPRs) at around 700 and 1100 nm is reported. By using UV–Vis–NIR absorption measurements and finite-difference time-domain calculations, the induction of the LSPR and the multipolar nature of the resonances have been investigated experimentally and theoretically. Simulation results demonstrate that large electric fields are confined at the tips of the branches, where the LSPR can be induced specifically by controlling the polarisation of the incident electric field. The surface-enhanced Raman scattering (SERS) capability of these dual plasmonic gold nanostars (DPGNS) has also been demonstrated using a Raman reporter, diethylthiatricarbocyanine iodide and high SERS enhancement factor (EF) of 2×10^7 is obtained with 785 nm excitation. With ease of synthesis, LSPR at NIR and high SERS EF, DPGNS demonstrated the capability to be an effective SERS substrate and the potential to elicit the highest SERS EF ever reported for gold nanoparticles, with further longer wavelength excitations at and beyond 1064 nm.

1. Introduction: When nanoscale metallic structures are excited by light at certain frequencies, the incident electric field induces waves of free electron oscillations confined to the nanostructure's surface; a phenomenon called localised surface plasmon resonance (LSPR) [1, 2]. The electromagnetic (EM) field distribution of the nanoparticle following the interaction with incident EM field can be obtained using quasi-static approximation when it is assumed that the nanoparticle is a homogeneous sphere and the size is much smaller than the excitation wavelength (radius $r \ll \lambda$). The phase of the surface plasmon oscillations are predominantly dipolar and are approximately constant over the nanoparticle's volume [1, 3]. The increase in the size of the nanoparticles has varying effects on LSPR and can be summarised as follows: (i) LSPR frequencies decrease (wavelength red-shift) with increasing size, (ii) LSPR dampens strongly, resulting in a dramatic decrease of the near-field intensity and (iii) appearance of new resonances that do not couple with light uniformly, as in smaller sized particles. When the nanoparticle's size becomes comparable to or larger than the wavelength of the incident light (radius $r \geq \lambda$), the conduction electrons at different locations in the nanoparticle can oscillate with the varying phases, resulting in excitation of higher-order multipolar modes such as quadrupole, octapole and so on [4–6].

Surface-enhanced Raman scattering (SERS) is one such plasmonic near-field enhanced process where the scattering cross-section of analytes is greatly enhanced when in resonance with the nanoparticle's LSPR frequency [4, 7]. One of the mechanisms for this enhancement process is called the EM enhancement, which involves intense localised surface plasmon electric fields on or between the nanoparticles' crevices and interstices, called hot-spots [1].

Gold nanorods and similar metal nanoparticles owe the majority of their local SERS enhancement to the presence of 'hot-spots' near the inter-particle gaps [7, 8]. An alternate way to enhance the localised plasmonic EM field is to increase the complexity of the nanoparticle's surface. Nanostructures with smooth surfaces, in isolation, display inferior field intensity at its surface compared with complex surfaces, with nanoprotrusions, due to the surface roughness, which enhances SERS signal [9, 10]. Gold nanostars, with their multibranched structure, can elicit significant enhancement at the tips without any induced aggregation due to the 'lightning rod' effect [7, 11]. Such multibranched nanoparticles (nanostars), with LSPR around 700 nm, were previously synthesised in our lab with the tips of the branches acting as hot-spots [12]. We have also reported preliminary data on extending the LSPR of the nanostar into the near infrared (NIR) region [13]. The objective of this Letter is to optimise the optical property of the nanostars in terms of controlling, tuning and characterising the LSPR bands experimentally and theoretically. Adjusting the gold precursor concentration with respect to the reducing agent as well as the reaction conditions, dual plasmonic gold nanostars (DPGNS) possessing two distinct LSPR bands with an increased number of branches and longer, sharper tips as compared with smaller nanostars [12] have been successfully synthesised. Finite-difference time-domain (FDTD) method has been further used to investigate the near-field and far-field properties of the DPGNS.

2. Materials and methods: The previously reported synthetic protocol [13, 14] was modified and further extended to simultaneously control the branch length and tip sharpness, which relates to the plasmon absorption in the NIR. An aqueous reaction

solution was first prepared by thoroughly mixing 400 µl of 10 mM of hydrogen tetrachloroaurate ($HAuCl_4$) and 40 µl of 10 mM silver nitrate ($AgNO_3$) in 20 ml deionised water. The concentration ratio of $HAuCl_4$:$AgNO_3$ was always maintained at 10:1. Then 80 µl of 100 mM reducing agent, ascorbic acid (AA), was added quickly under vigorous shaking. The colour of the reaction solution changed from colourless to reddish blue in 30 s, indicating the formation of DPGNS. Sample for SERS measurements was prepared by adding 166.6 µl of Raman reporter, diethylthiatricarbocyanine iodide (DTTCI), dissolved in dimethyl sulphoxide, drop-wise with 1 ml of DPGNS solution under vigorous stirring. UV–Vis absorption measurements were performed using a Shimadzu UV-2600 spectrometer. The nanoparticles' size and morphology was examined using a Hitachi H7000 and FEI Titan 80–300 kV transmission electron microscope (TEM). SERS measurements were carried out using a Renishaw Raman spectrometer with Invia microscope. The excitation source used was a 514 nm argon ion laser and 785 nm diode laser.

FDTD Solutions software (Lumerical Solutions Inc.) was used for computing near-field and far-field properties of the nanostars. DPGNS structure was modelled using dimensions measured from TEM images with water as the medium to replicate the synthesised DPGNS in aqueous solutions. Perfectly matched layers were used as boundaries and the incident source used was a total field scattered field source. The complex dielectric constants were obtained using the Johnson and Christy model [15]. Multiple three-dimensional power flow monitors were used to calculate the absorption and scattering cross-sections, near-field intensities and surface charge density analyses.

3. Results and discussion: A typical TEM image of the as-synthesised DPGNS clearly showed the multibranched structure of the nanostars with long branches and sharp tips (Fig. 1*a*). High-resolution TEM of the tip of a single branch and the corresponding fast Fourier transform (FFT) analysis (as shown in Fig. 1*b*) reveals the ⟨111⟩ growth direction of the tip and lattice spacing of 0.235 nm between the (111) planes, which is consistent with the previously synthesised nanostars with shorter branches [12, 16] and similar multibranched nanostructures [14, 17]. The absorption spectra of the as-synthesised DPGNS had two distinct SPR peaks; one in the visible region of the spectrum, called λ_1 hereon, and another in the NIR region, called λ_2 hereon; thus the name dual plasmonic gold nanostars. The intensity and position of both absorption peaks has been shown to be chemically controlled by adjusting the reaction parameters. Generation of λ_2 was carefully controlled by adjusting the concentration ratio of $HAuCl_4$ (gold precursor) and AA (reducing agent).

Fig. 1*c* shows the absorption spectra of samples with varying concentration ratios of $HAuCl_4$ and AA. It can be seen that the lowest AA concentration displayed only blue-shifted λ_1. Increased AA concentration did generate anisotropic multibranched morphology, with the concentration of 1.5 and 2 times that of $HAuCl_4$ displaying λ_2 at around 1100 and 1050 nm, respectively. Further increase in AA concentration not only led to the blue shift, but also a gradual disappearance of λ_2, with a concentration ratio of 1:3 resulting in only λ_1. The intensity of λ_1 can also be adjusted by varying the concentration ratio of $HAuCl_4$ to the total reaction volume [called dilution factor (DF)] and keeping the concentration of AA constant at 80 µM (Fig. 1*d*). Increasing DF (decreasing concentration of $HAuCl_4$ in the reaction volume) from 1:30 to 1:60 resulted in a gradual decrease in intensity of λ_1, which completely disappeared beyond the DF of 1:60. Varying the DF did not affect λ_2 significantly apart from minimal decrease in intensity with increasing DF.

To investigate the origins of λ_1 and λ_2 of the DPGNS, initially a single branch corresponding to one branch of the DPGNS was simulated. This was done to analyse the plasmon resonance associated with single tip and possible plasmon coupling with other tips of the DPGNS. During the simulation, the incident light source was set to be along the *z*-axis and the polarisation was varied from 90° in-plane (parallel to the axis of the branch) to 0° out-of-plane (perpendicular to the axis of the branch) polarisation angles. When exposed to in-plane polarisation (as seen in Fig. 2*a*), single branch of the DPGNS displayed plasmon

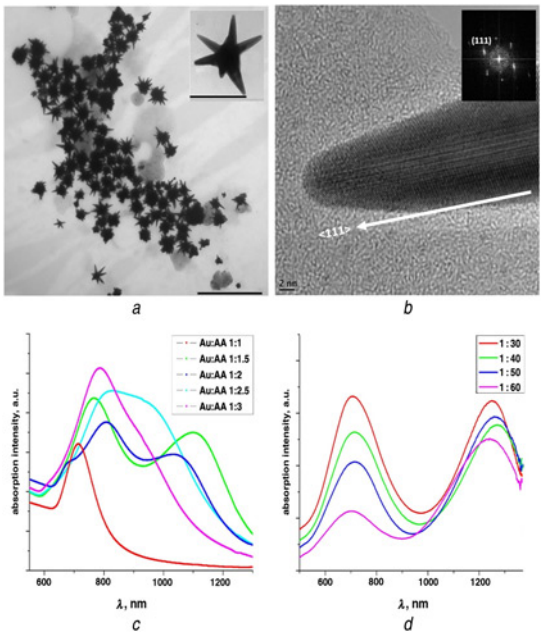

Fig. 1 *TEM image of DPGNS and absorption spectra*
a TEM image of DPGNS (scale bar – 500 nm) and inset showing high-magnification image of single DPGNS (scale bar – 100 nm)
b High-resolution TEM of the tip of a single branch and the corresponding FFT analysis (inset)
c Absorption spectra of various concentration ratios of gold precursor ($HAuCl_4$) and reducing agent (AA)
d Absorption spectra of various concentration ratios of gold precursor ($HAuCl_4$) to total reaction volume

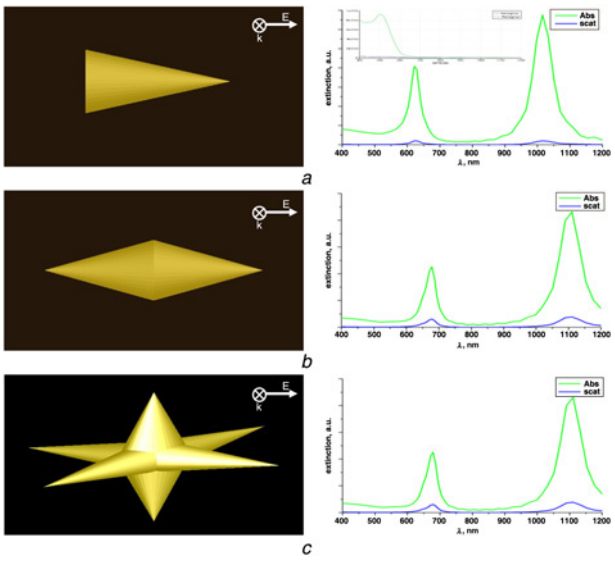

Fig. 2 *Simulated extinction spectra of*
a Single branch of DPGNS
b Double branches of DPGNS
c Multiple branches of DPGNS, excited with in-plane polarised source. The extinction spectrum when excited with out-of-plane polarisation was given as the inset in panel (*a*)

doi: 10.1049/mnl.2016.0095

absorption peaks at 625 and 1025 nm (corresponding to λ_1 and λ_2, respectively). This single tip in itself displayed superior LSPR properties, similar to high aspect ratio nanorods and nanodisks [3]. When two branches were placed adjacent to each other with no gap in-between (Fig. 2*b*), the dimer displayed λ_1 and λ_2 that were red-shifted to 685 and 1100 nm, respectively. The excitation resulted in the oscillation of conduction electrons between the two symmetric halves of the nanostructure, with the field intensity localised at the tips as a result of the spatial confinement of electrons to the smallest region of the nanostructure (tips of the branches in this case).

When multiple branches of same dimensions were simulated to resemble a DPGNS (Fig. 2*c*), the excitation with polarisation in-plane with the horizontal tips did not impart any changes to both λ_1 and λ_2. This implies that only the branches that are aligned in the polarisation direction of the incident field will give rise to significant localised field enhancement at the tips [18, 19]. This is also evidenced by the fact that excitation with out-of-plane polarisation only resulted in an absorption peak at around 520 nm and no resonance peak in the NIR region (inset of Fig. 2*a*). This peak arises from the spherical base of the cone-like structure in FDTD's object library used to model branches of the DPGNS. Unlike other star-shaped gold nanostructures that were reported to have multiple branches growing out a spherical core [3, 7, 11, 18, 19], DPGNS can be argued to not possess a spherical core of significant size. This is because none of the reaction parameters, shown in Figs. 1*c* and *d*, resulted in a resonance peak at around 520 nm, a characteristic of spherical gold nanoparticles

When a DPGNS with multiple branches is considered as a single nanostructure, its response to incident light can be classified based on the incident polarisation. Various polarisation angles excited plasmons of different tips at varying degrees, as demonstrated in the electric field enhancements (EFEs) ($|E|^2$) at the tips and corresponding extinction spectra in Fig. 3. The extinction spectra are characterised by two distinct peaks around 810 and 1100 nm and weaker features at around 610 and 685 nm.

Fig. 3*a* shows that with a polarisation angle of 90°, the extinction is dominated by a 810 nm plasmon resonance. Since this polarisation angle is in-plane with the vertical tips, the corresponding EFE image clearly shows the existence of large surface charges on the vertical tips.

At a polarisation angle of 60° (Fig. 3*b*), along with the 810 nm plasmon resonance, we can also notice a comparatively smaller resonance at 1100 nm. The corresponding EFE image shows that the plasmons on horizontal tips were also excited and showed localised field enhancements, although with less intensity compared with the vertical tips. It can be seen in Fig. 3*c* that the polarisation angle of 30° evoked an optical response from the DPGNS that is the reverse when excited at 60°; the existence of larger surface charges on the horizontal tips compared with smaller enhancement on the vertical tips. A corresponding extinction spectrum shows a new resonance at 685 nm, along with a larger resonance at 1100 nm and a smaller resonance at 810 nm. The resonance at 810 nm completely disappears at a polarisation angle of 0° (Fig. 3*d*), with bands peaking only at 685 and 1100 nm (λ_1 and λ_2, respectively). Its corresponding EFE image shows intense local field enhancement only on the horizontal tips, similar to Fig. 2*c*.

In brief, the horizontal tips were the origin for resonance peaks at 685 and 1100 nm, and the resonance peaks at 600 and 810 arises from vertical tips. As the polarisation angle was changed from 90 to 0°, the intensities of 685 and 1100 nm peaks gradually increased, while the intensities of 600 and 810 nm peaks gradually decreased. The corresponding electric field intensity images confirmed this pattern with the localised field intensities of horizontal tips gradually increasing and localised field intensities of the vertical tips gradually decreasing, when the incident polarisation angle was changed from 90 to 0°. This polarisation dependence of the LSPR has also been found in other anisotropic nanostructures, like nanocrescents

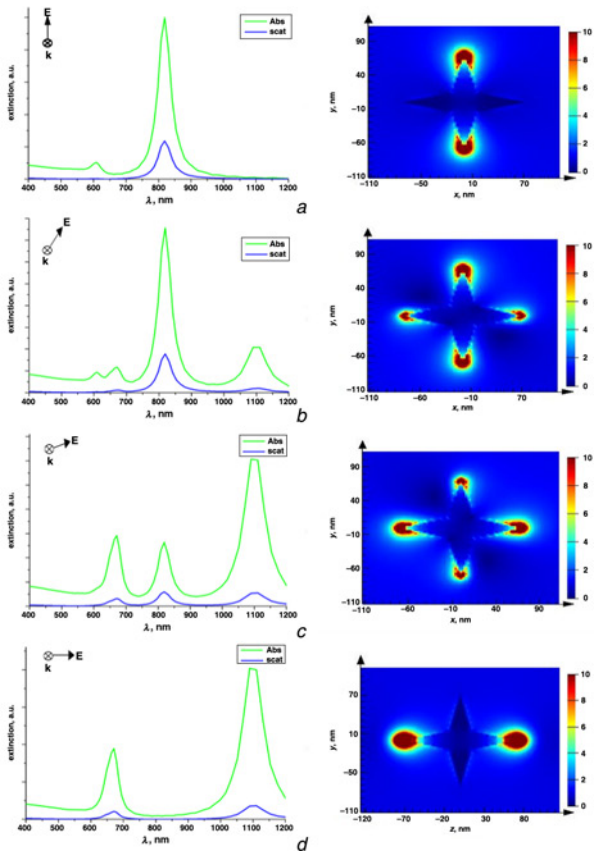

Fig. 3 *Extinction spectra and corresponding EFE images of DPGNS excited by incident light with different polarisations*
a 90°
b 60°
c 30°
d 0°

[3, 20] and nanoprisms [21]. The results indicate that each tip in the DPGNS has a certain orientation, and the spectral peaks are the collective result of plasmon resonances of multiple tips with distinct resonance wavelengths. Thus, using polarised light, it is possible to specifically excite any of the resonance peaks of DPGNS.

Since colloidal DPGNS is a heterogeneous sample (varying in number and orientation of tips), the wavelength position and relative intensity of the resonance peaks suggest that λ_1 is the sum of 600, 685 and 810 nm peaks [11]. DPGNS in aqueous solutions are not macroscopically oriented within the solvent and thus we can observe only the average over all possible orientations with both λ_1 and λ_2 appearing in the absorption spectrum [5, 11]. It can also be seen that the extinction of DPGNS is dominated by absorption. This high absorption cross-section of DPGNS makes it an efficient antenna for exciting the analytes on its vicinity and absorbing the energy from the near-field emitted by those analyte molecules and radiate into the far-field [22].

The presence of multiple resonance peaks when excited with the incident light of different polarisation angles can be analysed using the multipolar resonance concept. The consensus on the optical response of metallic nanoparticles, in terms of LSPR, is determined by the relative dimension of the particle with respect to the wavelength of the incident radiation [1, 5, 23]. Particles would exist in a uniform field when its dimension is much smaller than the wavelength of light. Thus, the conduction electrons experience similar phase effects and oscillate in only one direction, creating a dipole. When the size of the particle increases, the particle will not experience uniform electric field and the incident light cannot polarise on the particle homogeneously. As a consequence, the

dipole is not the only mode of resonance anymore, and the particle's resonance band splits into multiple peaks generated by multipolar modes. The three resonance peaks of DPGNS at 1100, 810 and 685 nm that exist at different intensities can be attributed to dipole, quadrupole and octapole modes, respectively. The charge density distribution calculated at each of those resonant wavelengths are given in Figs. 4*a*–*c* that shows distinct areas of charge separation, which demonstrates plasmon resonance characteristics of dipole (two), quadrupole (four) and octapole (eight) modes.

The SERS capability of DPGNS was then investigated. One key factor in explaining the SERS capability of any nanostructure is its SERS enhancement factor (EF). For the theoretical calculation of SERS EF, a linear simulation was run in FDTD using electric field profile monitors to measure the field intensity with an analytical script specific for calculating the EF = $(E/E_0)^4$. The EF images of the DPGNS at three different wavelengths corresponding to the multipolar modes discussed earlier are shown in Figs. 4*d*–*f*. It is well known that the intensity of higher-order modes is lesser than lower-order modes [6], which means that the EFE is also lesser in intensity for higher-order modes. This proves to be the case with DPGNS, with the dipole mode being excited at 1100 nm (Fig. 4*d*) showing the highest EF ($|E|^4$) of 2.4×10^7, followed by the quadrupole mode (Fig. 4*e*) being excited at 810 nm and the octapole mode (Fig. 4*f*) at 685 nm. Due to the inhomogeneous number of branches on DPGNS and the huge difficulty in sustaining higher-order plasmon modes, the octapole mode is hardly proven by experimental results [21].

The longer the branches and the sharper the tips of the nanostar, the more is the red-shift of the LSPR, leading to a more intense localised field intensity at the tips [16]. The localised electric field intensity of the DPGNS should be more intense than similar nanostructures with shorter branch lengths and tips with higher apex angles [3, 11]. To confirm this, SERS spectrum of a Raman reporter, DTTCI, coated onto DPGNS was acquired (Fig. 5). SERS by DPGNS was compared with previously synthesised nanostars, which possessed shorter branches and tips with higher apex angles (inset in Fig. 5) [12]. The Raman signal enhancement by DPGNS was more than twice that of the enhancement by nanostars, displaying the predominance of the EM mechanism towards SERS [1] because of the highly intense localised field intensity at the tips of longer and sharper branches of the DPGNS. The chemical enhancement for SERS arises principally through the charge

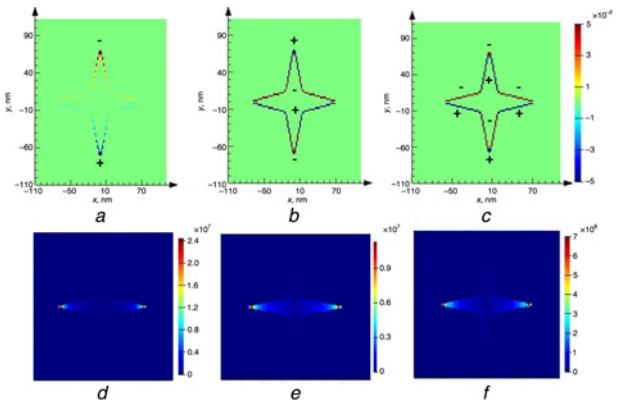

Fig. 4 *Charge density distributions on DPGNS's surface displaying multipolar plasmon resonance modes at resonant wavelengths*
a Dipole at 1100 nm
b Quadrupole at 810 nm
c Octapole at 685 nm
SERS EF of the DPGNS at multiple plasmon resonance modes
d Dipole mode showing the maximum EF excited at 1100 nm
e Quadrupole mode excited at 810 nm
f Octapole mode excited at 685 nm

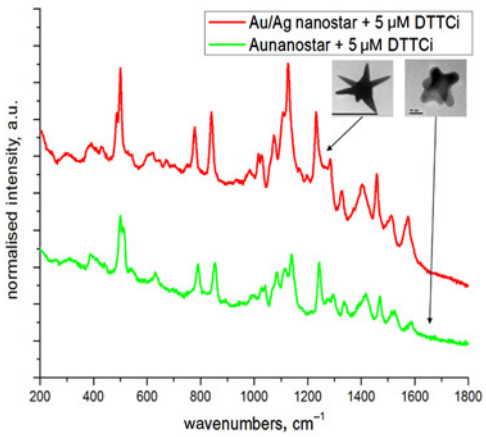

Fig. 5 *Raman spectra of 5 μM DTTCI enhanced by DPGNS and nanostar (insets showing the corresponding TEM images), when excited at 785 nm*

transfer mechanism that relies on the surface energy of the crystal planes and stronger Raman enhancement is observed for (100) and (110) planes than (111) [9, 24]. Though smaller nanostars and DPGNS possess branches with ⟨111⟩ growth direction, DPGNS displayed superior SERS due to larger surface area and higher number of hot-spots [9].

The experimental SERS EF was calculated using the following equation [25, 26]

$$\text{SERS EF} = \frac{I_{\text{SERS}}/C_{\text{SERS}}}{I_{\text{RS}}/C_{\text{RS}}} \tag{1}$$

In (1), I_{RS} and C_{RS} are the Raman signal intensity and concentration of analyte molecules under non-SERS condition (in the absence of gold nanosubstrate), respectively, and I_{SERS} and C_{SERS} are the Raman intensity and molar concentration of the analyte molecules involved in SERS process (in the presence of gold nanosubstrate), respectively. Since the experimental parameters (including reporter concentration, gold concentration in nanostars, laser power, acquisition time and depth of focus) are all kept constant, the relative intensity of the signature Raman peak of DTTCI at 1128 cm^{-1} was used to calculate SERS EF. The experimental EF of nanostars and DPGNS at two different laser wavelengths are summarised in Table 1.

The SERS EF of DPGNS is understandably higher than nanostars, and is also comparable to the computed theoretical EF (Fig. 4). The EF of DPGNS at the excitation wavelength of 785 nm is the highest measured for similarly reported anisotropic gold nanostructures with inherent hot-spots [7, 22]. Though the SERS enhancement by the nanostars was inferior compared with DPGNS, it was still better than other anisotropic nanostructures like nanorods and nanospheres. Samanta *et al.* [26] compared the SERS EF of nanostars, synthesised using a seed-mediated nucleation and growth protocol with broad LSPR band in the range of 600–900 nm, and similar sized nanorods and nanospheres. Using similar experimental parameters, their study reported nanostars

Table 1 SERS EF of nanostars and DPGNS at 514 and 785 nm excitation wavelengths

Nanostructures	SERS EF	
	514 nm ($\times 10^5$)	785 nm ($\times 10^7$)
nanostars	0.9	0.059
DPGNS	1.8	2

doi: 10.1049/mnl.2016.0095

to exhibit the highest SERS EF followed by nanorods and nanospheres.

FDTD simulation of two adjacently placed DPGNS structures with inter-particle distances from 0–10 nm displayed no red-shifting of the either λ_1 or λ_2. This might be counterintuitive considering that the plasmon coupling of adjacent nanostructures has been proven in nanodisks, nanoshells and so on [3, 20]. However, this plasmon coupling occurs when the dipole of a nanostructure is in symmetry with the neighbouring dipole. Most of the studies reporting a higher EFE through plasmon coupling used an array of nanostructures carefully positioned adjacent to each other transversally or longitudinally (side-by-side or lengthwise, respectively) [3, 4, 27, 28]. Thus, for the incident light polarisation along the inter-particle axis, the interaction between the dipoles is positive, which leads to the red-shift in their LSPR in the dimers. DPGNS in solution are aligned randomly, meaning most of the dipoles on the tips would be asymmetrical to each other and thus the interaction will be repulsive [4]. This further reiterates that DPGNS possess inherent hot-spots with enhanced field intensities compared with nanorods, nanoshells and nanodisks that depend on the inter-particle sites for field intensity enhancement [3, 4, 7].

Studies have shown that it is critical to have the incident laser frequency overlapping the frequency with maximum plasmon resonance energy [7, 29]. SERS EF has been shown to increase dramatically when the laser frequency and LSPR frequency approach the NIR region. It can be seen from Table 1 that the EF values of both nanostars and DPGNS are higher at 785 nm excitation than at 514 nm. Though the LSPR of nanostar ($\simeq$665 nm) and λ_1 of DPGNS lie closer to each other, the resonance peak (770 nm) of the Raman reporter lies closely to the excitation laser wavelength (785 nm), inducing the resonance Raman condition [30, 31], and thus a higher Raman enhancement compared with laser excitation wavelength of 514 nm.

It is also interesting to note that even though both nanostars and DPGNS had LSPR close to 785 nm, DPGNS displayed an EF that is dramatically higher than the nanostar at 785 nm excitation (see Table 1). This can be explained by the fact that the lightning rod effect would be more pronounced with increasing length of the branches and sharpness of the tips [32, 33]. Theoretical calculations have shown that the increase in length and sharpness of the nano-protrusions does not only cause a red-shift, but also increases the intensity of the LSPR [16]. This effect is the result of an increased spatial confinement of the electrons on the sharpest tips or crevices within the nanostructure, increasing the energy of the plasmon resonance, and thus intensifying the local EFE. Though the option is not available with our current in-house Raman measurement setup, the SERS EF of DPGNS at the excitation wavelength of 1064 nm (closely matching λ_2 of DPGNS) would theoretically be higher than the EF obtained with 785 nm excitation. This is because the NIR excitation at a longer wavelength should induce a local EFE at higher intensities, and thus a larger SERS cross-section [29, 34].

4. Conclusion: DPGNS displayed LSPR at two distinct wavelengths, one in the red region around 700 nm and another in the NIR region around 1100 nm. The experimental results indicate that the wavelength shifts and intensities of the LSPR can be carefully controlled by adjusting the concentrations of gold precursor and reducing agent in the reaction solution. FDTD simulations were performed to investigate specific induction of different plasmon resonance modes of the DPGNS by controlling the incident polarisation. These plasmon resonance modes can be excited at distinct wavelengths and were spectrally well resolved. FDTD analysis of the surface charge distribution investigation showed the multipolar nature of the LSPR bands with dipole resonance being the dominant mode in the NIR region, followed by quadrupole and octapole modes, in the far-red and red region of the spectrum, respectively. Manipulation of the localised electric field distribution by light polarisation enhanced DPGNS's SERS capability. DPGNS exhibited superior SERS EF of 2×10^7 (with 785 nm excitation), much higher than that of nanostars with smaller branches and less sharper tips. The results showed the potential of DPGNS to elicit the highest SERS EF ever reported for colloidal gold nanoparticles with longer wavelength excitations at and beyond 1064 nm.

5. Acknowledgments: This work was supported by the Science Foundation Ireland (SFI). Authors thank Dr Alan Casey of the Nanolab Research Centre at Dublin Institute of Technology for helping in measuring the elemental concentrations of DPGNS using AAS.

6 References

[1] Etchegoin P.G., Le Ru E.C.: 'Basic electromagnetic theory of SERS', 2011, pp. 1–37
[2] Kelly K.L., Coronado E., Zhao L.L., *ET AL.*: 'The optical properties of metal nanoparticles: the influence of size, shape, and dielectric environment', *J. Phys. Chem. B*, 2003, **107**, (3), pp. 668–677
[3] Chung T., Lee S.-Y., Song E.Y., *ET AL.*: 'Plasmonic nanostructures for nano-scale bio-sensing', *Sensors*, 2011, **11**, (11), pp. 10907–10929
[4] Jain P.K., El-Sayed M.A.: 'Plasmonic coupling in noble metal nanostructures', *Chem. Phys. Lett.*, 2010, **487**, (4), pp. 153–164
[5] Garcia M.: 'Surface plasmons in metallic nanoparticles: fundamentals and applications', *J. Phys. Appl. Phys.*, 2011, **44**, (28), p. 283001
[6] You E.-A., Zhou W., Suh J.Y., *ET AL.*: 'Polarization-dependent multipolar plasmon resonances in anisotropic multiscale Au particles', *ACS Nano*, 2012, **6**, (2), pp. 1786–1794
[7] Samanta A., Maiti K.K., Soh K., *ET AL.*: 'Ultrasensitive near-infrared Raman reporters for SERS-based in vivo cancer detection', *Angew. Chem. Int. Ed.*, 2011, **50**, (27), pp. 6089–6092
[8] Tian F., Bonnier F., Casey A., *ET AL.*: 'Surface enhanced Raman scattering with gold nanoparticles: effect of particle shape', *Anal. Methods*, 2014, **6**, (22), pp. 9116–9123
[9] Bechelany M., Brodard P., Elias J., *ET AL.*: 'Simple synthetic route for SERS-active gold nanoparticles substrate with controlled shape and organization', *Langmuir*, 2010, **26**, (17), pp. 14364–14371
[10] Sakamoto S., Philippe L., Bechelany M., *ET AL.*: 'Ordered hexagonal array of Au nanodots on Si substrate based on colloidal crystal templating', *Nanotechnology*, 2008, **19**, (40), p. 405304
[11] Nehl C.L., Liao H., Hafner J.H.: 'Optical properties of star-shaped gold nanoparticles', *Nano Lett.*, 2006, **6**, (4), pp. 683–688
[12] Raghavan V., Connolly J.M., Fan H.M., *ET AL.*: 'Gold nanosensitisers for multimodal optical diagnostic imaging and therapy of cancer', *J. Nanomed. Nanotechnol.*, 2014, **5**, (6), p. 1
[13] Raghavan V., Subhash H., Breathnach A., *ET AL.*: 'Dual plasmonic gold nanoparticles for multispectral photoacoustic imaging application'. Int. Society for Optics and Photonics, 2014, p. 89434J-1–89434J-13
[14] Cheng L.-C., Huang J.-H., Chen H.M., *ET AL.*: 'Seedless, silver-induced synthesis of star-shaped gold/silver bimetallic nanoparticles as high efficiency photothermal therapy reagent', *J. Mater. Chem.*, 2012, **22**, (5), pp. 2244–2253
[15] Johnson P.B., Christy R.-W.: 'Optical constants of the noble metals', *Phys. Rev. B*, 1972, **6**, (12), p. 4370
[16] Cai J., Raghavan V., Bai Y.J., *ET AL.*: 'Controllable synthesis of tetrapod gold nanocrystals with precisely tunable near-infrared plasmon resonance towards highly efficient surface enhanced Raman spectroscopy bioimaging', *J. Mater. Chem. B*, 2015, **3**, (37), pp. 7377–7385
[17] Xie J., Lee J.Y., Wang D.I.: 'Seedless, surfactantless, high-yield synthesis of branched gold nanocrystals in HEPES buffer solution', *Chem. Mater.*, 2007, **19**, (11), pp. 2823–2830
[18] Hao F., Nehl C.L., Hafner J.H., *ET AL.*: 'Plasmon resonances of a gold nanostar', *Nano Lett.*, 2007, **7**, (3), pp. 729–732
[19] Khoury C.G., Vo-Dinh T.: 'Gold nanostars for surface-enhanced Raman scattering: synthesis, characterization and optimization', *J. Phys. Chem. C*, 2008, **112**, (48), pp. 18849–18859
[20] Wu L.Y., Ross B.M., Lee L.P.: 'Optical properties of the crescent-shaped nanohole antenna', *Nano Lett.*, 2009, **9**, (5), pp. 1956–1961
[21] Li Z., Yu Y., Chen Z., *ET AL.*: 'Ultrafast third-order optical nonlinearity in Au triangular nanoprism with strong dipole and quadrupole plasmon resonance', *J. Phys. Chem. C*, 2013, **117**, (39), pp. 20127–20132
[22] Moskovits M.: 'Persistent misconceptions regarding SERS', *Phys. Chem. Chem. Phys.*, 2013, **15**, (15), pp. 5301–5311

[23] Khlebtsov N.G., Dykman L.A.: 'Plasmonic nanoparticles: fabrication, optical properties, and biomedical applications', in Tuchin V.V. (Ed.): 'Handbook of photonics for biomedical science' (CRC Press, Boca Raton, FL, 2010), pp. 37–82
[24] Nikoobakht B., Wang J., El-Sayed M.A.: 'Surface-enhanced Raman scattering of molecules adsorbed on gold nanorods: off-surface plasmon resonance condition', *Chem. Phys. Lett.*, 2002, **366**, (1–2), pp. 17–23
[25] Le Ru E.C., Blackie E., Meyer M., *ET AL.*: 'Surface enhanced Raman scattering enhancement factors: a comprehensive study', *J. Phys. Chem. C*, 2007, **111**, (37), pp. 13794–13803
[26] Samanta A., Jana S., Das R.K., *ET AL.*: 'Wavelength and shape dependent SERS study to develop ultrasensitive nanotags for imaging of cancer cells', *RSC Adv.*, 2014, **4**, (24), p. 12415
[27] Jain P.K., El-Sayed M.A.: 'Noble metal nanoparticle pairs: effect of medium for enhanced nanosensing', *Nano Lett.*, 2008, **8**, (12), pp. 4347–4352
[28] Acimovic S.S., Kreuzer M.P., González M.U., *ET AL.*: 'Plasmon near-field coupling in metal dimers as a step toward single-molecule sensing', *ACS Nano*, 2009, **3**, (5), pp. 1231–1237
[29] Greeneltch N.G., Blaber M.G., Schatz G.C., *ET AL.*: 'Plasmon-sampled surface-enhanced Raman excitation spectroscopy on silver immobilized nanorod assemblies and optimization for near infrared (λex = 1064 nm) studies', *J. Phys. Chem. C*, 2012, **117**, (6), pp. 2554–2558
[30] McNay G., Eustace D., Smith W.E., *ET AL.*: 'Surface-enhanced Raman scattering (SERS) and surface-enhanced resonance Raman scattering (SERRS): a review of applications', *Appl. Spectrosc.*, 2011, **65**, (8), pp. 825–837
[31] Schatz G.C., Young M.A., Van Duyne R.P.: 'Electromagnetic mechanism of SERS', in Kneipp K., Moskovits M., Kneipp H. (Eds): 'Surface-enhanced Raman scattering' (Springer, 2006), pp. 19–45
[32] Le F., Brandl D.W., Urzhumov Y.A., *ET AL.*: 'Metallic nanoparticle arrays: a common substrate for both surface-enhanced Raman scattering and surface-enhanced infrared absorption', *ACS Nano*, 2008, **2**, (4), pp. 707–718
[33] Liao P., Wokaun A.: 'Lightning rod effect in surface enhanced Raman scattering', *J. Chem. Phys.*, 1982, **76**, (1), pp. 751–752
[34] Kearns H., Shand N., Smith W., *ET AL.*: '1064 nm SERS of NIR active hollow gold nanotags', *Phys. Chem. Chem. Phys.*, 2015, **17**, (3), pp. 1980–1986

doi: 10.1049/mnl.2016.0095